ISSN: 2621-4709 E-ISSN: 2621-2528
Journal of Applied Agricultural Science and Technology
Vol. 10 No. 2 (2026): 276-297

Land-Use Scenario Modeling Using Remote Sensing and Cellular Automata and Its Impact on the Drought Hazard at the Sub-catchment Area Level

Suryanta Junjungan Tua Sitio [a], Novandi Rizky Prasetya [b], Michelle Talisia Sugiarto [b], Aditya Nugraha Putra [c,d,*]

[a] Agroecotechnology Study Program, Faculty of Agriculture, Brawijaya University, Malang, Indonesia
[b] Soil and Water Management Study Program, Faculty of Agriculture, Brawijaya University, Malang, Indonesia
[c] Department of Soil Science, Faculty of Agriculture, Brawijaya University, Malang, Indonesia
[d] Department of Land and Water Resources Management, Faculty of Civil Engineering, Slovak University of Technology, Bratislava, Slovakia

Abstract. *Rapid land-use change in upland watersheds alters hydrological processes and increases drought vulnerability. The Upper Brantas and Kali Konto sub-watersheds in East Java serve as important rainfall catchment and water storage areas, yet ongoing land conversion has progressively reduced their capacity to regulate water availability. However, the implications of future land-use trajectories for drought hazards at the sub-catchment scale remain insufficiently understood. This study aims to analyze land-use dynamics, simulate future land-use change, and evaluate alternative land-use planning scenarios to assess their potential influence on drought hazard distribution. Multi-temporal land-use data from 2017, 2019, 2021, and 2025 were analyzed using remote sensing, and future land-use patterns were projected for 2030 using the Artificial Neural Network–Cellular Automata–Markov (ANN–CA–Markov) model. The simulated land-use distribution was then evaluated under Regional Spatial Planning (RSP) and Land Capability Classification (LCC) scenarios to examine their implications for drought hazards. The results showed a substantial decline in natural forest from 12,600.35 ha (31.4%) in 2017 to 9,975.70 ha (24.9%) in 2025—a reduction of more than 20%—accompanied by the expansion of plantation systems, dryland farming, and built-up areas. Under the 2030 Business-as-Usual (BAU) scenario, moderate drought hazard areas increased from 44.0% to approximately 50.2% of the watershed area. Among the evaluated scenarios, the Land Capability Classification (LCC)-based planning approach showed the greatest potential to mitigate drought risk, reducing high drought hazard areas from 25.1% under the BAU scenario to 15.2%. These findings highlight the importance of integrating land capability considerations into spatial planning to support drought-resilient watershed management.*

Keywords: *drought; land cover; landscape; machine learning; remote sensing.*

Type of the Paper: Regular Article.

1. Introduction

Prolonged moisture deficits that reduce water availability in soils and vegetation pose increasing risks to tropical watersheds, particulary where rapid land-use change has altered hydrological functions [1]. Indonesia lost approximately 32 million hectares of tree cover between

https://doi.org/10.55043/jaast.v10i2.467
Received June 16, 2025; Received in revised form August 03, 2026; Accepted April 9, 2026; **ARTICLES IN PRESS**
* First corresponding author
Email: aditya.n.putra@ub.ac.id

2001 and 2024, with 1.5 million hectares of natural forest disappearing between 2021 and 2024 alone [2]. In East Java, several districts have experienced severe drought events, with more than 60 consecutive days without significant rainfall recorded in some locations [3]. This trends are not coincidental: deforestation and land-use conversion in upstream areas reduce infiltration capacity and soil moisture retention, thereby altering catchment hydrology and increasing drought vulnerability [4]. Understanding this linkage is critical for the Upper Brantas and Kali Konto sub-watersheds, which function as key rainfall catchment and water storage areas but have experienced progressive land conversion over the past decade

Covering approximately 40,943.50 ha, the Upper Brantas and Kali Konto sub-watersheds serve as critical rainfall catchment and water storage areas in East Java [5]. However, ongoing land-use conversion has progressively reduced the effectiveness of water catchment functions, leading to declining spring discharge and availability [6]. Population growth and deteriorating environmental quality further exacerbated these hydrological changes [7]. Studies in the Upper Brantas watershed indicate that forest encroachment and inappropriate upstream land use have accelerated watershed degradation, reducing water availability and disrupting watershed functions [8]. Furthermore, deforestation increases the risk of hydrological disasters, including drought [9]. In the Brantas–Metro groundwater basin, which includes the Malang and Batu areas, evidence indicates severe aquifer stress and declining groundwater availability. These conditions have forced local residents to rely increasingly on piped water systems.

In principle, Regional Spatial Planning (RSP) integrates social, economic, and environmental considerations—including land capability analysis—to guide land-use allocation [10]. However, current RSP implementation often prioritizes economic development, and its effectiveness in reducing drought risk has not been systematically evaluated. This study evaluates drought hazard using a multi-parameter approach that integrates annual rainfall, dry months, evapotranspiration, land use, geology, water use intensity, and specific water discharge. This approach allows a spatial assessment of drought vulnerability at the sub-catchment level [11]. These knowledge gaps highlight the need to integrate remote sensing and land-use change modeling to improve spatial drought analysis [12]. Previous studies have primarily focused on historical or present drought conditions, with limited analysis of future drought scenarios at the regional scale. Moreover, the implications of alternative land-use planning strategies, such as Regional Spatial Planning (RSP) and land capability-based land allocation, for drought mitigation remain insufficiently explored.

This study combines multiple land-use scenarios—baseline (business-as-usual, BAU), Regional Spatial Planning (RSP), and Land Capability Class (LCC)—with remote sensing and

ANN–CA–Markov modeling to simulate future land-use change and evaluate its impact on drought hazard. This research projects future drought hazards under different planning scenarios, enabling proactive land management strategies. The ANN–CA–Markov model enables spatial simulation of land-use change, while scenario-based drought evaluation provides insights for watershed planning and management. The predicted land use is then compared with the 2030 Regional Spatial Planning (RSP) and Land Capability Class (LCC) scenarios to evaluate their implications for drought hazard at the sub-catchment scale.

2. Materials and Methods

2.1 Research Location

The Sumber Brantas and Kali Konto sub-watershed are part of the Brantas watershed and located at elevations ranging from 1,000 and 3,000 meters above sea level (m.a.s.l), as shown in Fig. 1. The Sumber Brantas and Kali Konto sub-watersheds are located between coordinates 645,870.190 – 675,223.961 East and 9,143,485.061 – 9,121,138.608 South.

Administratively, the Sumber Brantas and Kali Konto sub-watersheds cover parts of Batu City, Malang Regency, Pasuruan Regency, Mojokerto Regency, Jombang Regency, and Blitar Regency. The Kali Konto sub-watershed specifically covers parts of Malang Regency, Jombang Regency, and Blitar Regency. The Sumber Brantas sub-watershed is dominated by annual rainfall exceeding 2,000 mm, while The Kali Konto sub-watershed receives approximately 1,501 mm of rainfall per year. Rainfall deficits may lead to prolonged dry seasons that increase the likelihood of drought events [13].

Land usein the Sumber Brantas and Kali Konto sub-watersheds is dominated by agriculture (approximately 50%), including moorland, rice fields, and plantations Natural Forest areas generally have lower drought vulnerability, whereas residential and agricultural areas tend to be more prone to drought due to higher water demand and reduced water availability. The geological structures of the Sumber Brantas and Kali Konto sub-watershed areas are dominated by volcanic formations. The geological formations in the Sumber Brantas and Kali Konto sub-watershed include Qvaw (Arjuno Welirang volcanic rocks), Qpat (Anjasmara volcanic rocks), Qvp (Panderman volcanic rocks), Qpvkb (Kawi-Butak volcanic rocks), and Qpva (young Anjasmara volcano rocks) [13].

The Sumber Brantas and Kali Konto sub-watersheds experience 5-7 dry months annually, with evapotranspiration ranging from 750–1,500 mm per year, resulting in several areas that are vulnerable to droughts [13]. Thus, climate variability, land use, and geological factors strongly influence hydrological conditions in the watershed.

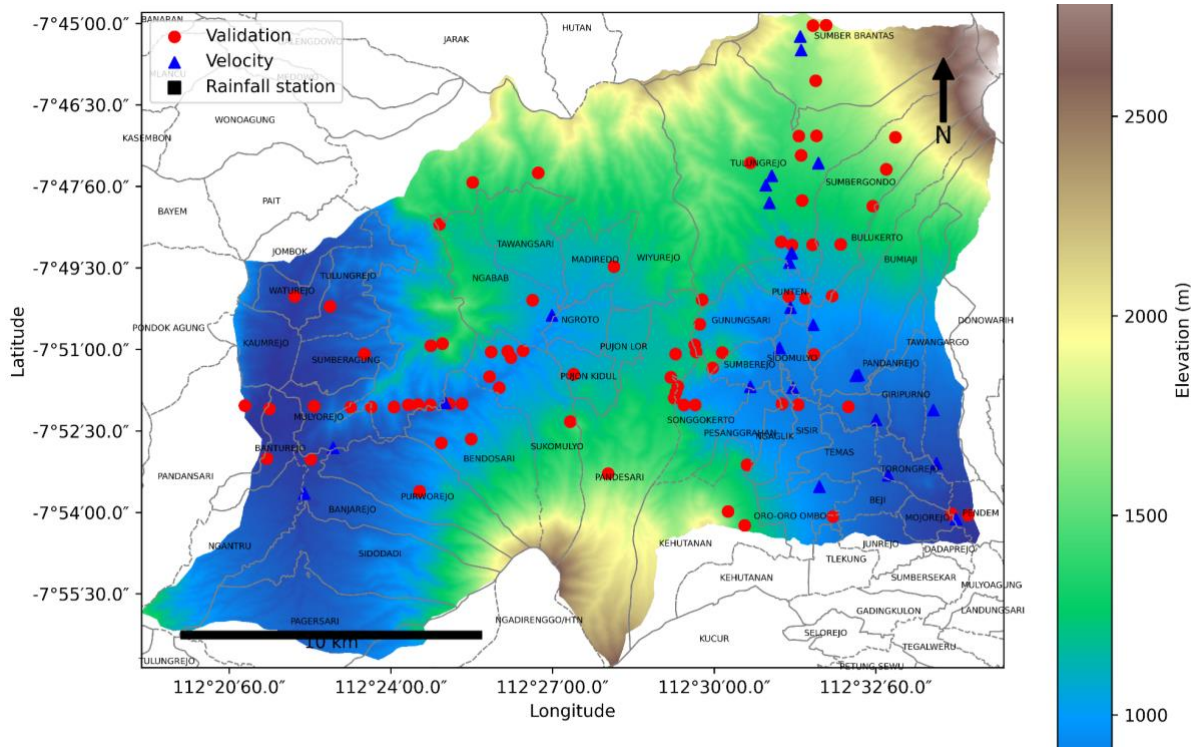

Fig. 1. Location of the Sumber Brantas and Kali Konto sub-Watersheds within the Upper Brantas Watershed, East Java, Indonesia.

2.2 Conceptual Framework

This research aims to identify the most suitable land-use scenario to reduce drought risk and mitigate future drought hazards. Drought occurrence is influenced by several factors, including land use, water demand, climate conditions, and natural environmental characteristics. Land use significantly influenceswater availability and drought vulnerability within a watershed (Fig. 2).

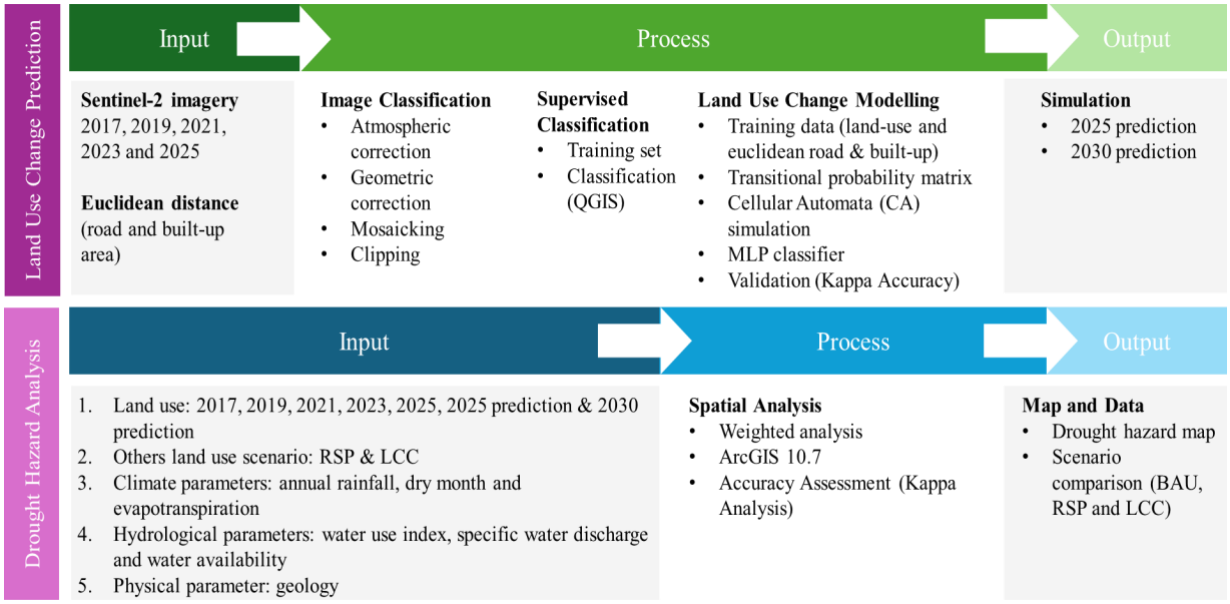

Fig. 2. Conceptual framework of land-use change modeling and drought hazard assessment using the ANN–CA–Markov approach and scenario-based land management analysis.

The conceptual framework of this study integrates land-use change modeling with drought hazard assessment to evaluate the potential impacts of different land-use management strategies. Historical land-use data derived from satellite imagery for 2017, 2019, 2021, 2023, and 2025 are used to analyze land-use dynamics. An ANN–CA–Markov model is applied to simulate land-use change and predict future land-use patterns. The model first generates a prediction for 2025, which is then compared with the classified land-use map of the same year to evaluate model performance. After validation, the model is used to simulate land-use conditions for 2030.

The predicted land-use scenario is subsequently compared with alternative land-use planning scenarios, including the Business as Usual (BAU) scenario, the Regional Spatial Planning (RSP) 2030 scenario, and the Land Capability (LC) scenario. Drought hazard maps are generated using a weighted overlay approach in a geographic information system (GIS), integrating several environmental parameters related to drought occurrence. The comparison of these scenarios provides a basis for identifying the most appropriate land-use management strategy to reduce future drought risk.

2.3 Land Use Analysis

2.3.1 Sentinel 2A Imagery Acquisition

The study used Sentinel 2A imagery acquired in 2017, 2019, 2021, 2023, and 2025, obtained from the Copernicus Open Access Hub (https://scihub.copernicus.eu/). The imagery was selected based on the study area coverage and cloud cover conditions.

2.3.2 Sentinel 2A Imagery Preprocessing

Sentinel 2A image preprocessing included atmospheric, radiometric, geometric corrections, as well as cloud removal [14]. Preprocessing was conducted using QGIS software with the Semi-Automatic Classification Plugin (SCP). The preprocessing steps included DOS1 atmospheric correction, bandset creation, and bandset processing using the SCP tools. Geometric correction was performed using the GDAL Georeferencer plugin in QGIS, where ground control points aligned the satellite imagery with spatial reference data. A first-order polynomial transformation with nearest-neighbor resampling was applied during the geometric correction. Cloud and haze effects were further reduced using PCI Geomatica software to improve image quality for subsequent analysis [15].

2.3.3 Supervised Classification

Land use classification employed a supervised classification approach in ArcGIS 10.7, using polygons to generate training sample datasets. Training samples created spectral signatures for each land-use class. Spatial Analyst tools and high-resolution imagery from Google Earth

assisted the interpretation of land-use classes, including protected forest, production forest, shrub, rice field and moor, residential areas, water bodies, and vacant land [16].

2.4 Land Use Scenario

2.4.1 Preparation of Land Use Map Using CA-ANN

To develop a land-use prediction model, road networks and built-up area data were obtained from the Indonesian Geospatial Portal (https://tanahair.indonesia.go.id/). Built-up areas were extracted from the land-use classification results. The downloaded spatial data were clipped to the boundaries of the Sumber Brantas and Kali Konto sub-watersheds. Built-up areas were then selected using attribute queries and exported as separate spatial layers. The Euclidean Distance tool generated raster layers representing the distance to built-up areas. Land-use change modeling was conducted using the ANN–CA–Markov approach implemented in the MOLUSCE plugin in QGIS. Land-use classifications from 2017 and 2021 simulated land-use change and generated a predicted land-use map for 2025 [17]. An MLP classifier with 300 iterations and kappa analysis was used for data validation complementing the transition matrix analysis [18].

2.4.2 Preparation of Land Use Map Based On Regional Spatial Planning (RSP)

The Regional Spatial Planning (RSP) map for 2030 for Batu City and Malang Regency was obtained and georeferenced, then converted into land-use classes consistent with the classification scheme used in this study. Table 1 presents the land-use conversion based on the RSP map.

Table 1. Conversion

No.	RSP	LULC
1	River, Cistern, Lake	Body of Water
2	Protected Forest, Forest Park	Natural Forest
3	Production Forest	Production Forest
4	Tourism Area, Public Services Area, Office Area, Residential Area, Urban Area, Trading Area, Cable Car Station, Sub-Cable Car Station, Industry, Agricultural Area, Production Land	Built-up Area
5	Production Land	Production Land
6	Green Space Area	Modified Forest
7	Rice Field, Irrigation Area	Rice Field
8	Moor	Moor

2.4.3 Preparation of Land Use Map Based on Land Capability Class (LCC)

Land Capability Class (LCC) maps were generated by comparing limiting land factors with the classification criteria proposed by Quandt et al. [19], using land system maps at a scale of 1:50,000.

2.5 Analysis of Management Factors and Driving Factors

A drought hazard map was developed by integrating several parameters based on the approach proposed by Paimin et al. [20], including annual rainfall, land use, dry months, geology,

water use index, specific water discharge, and annual evapotranspiration. The scoring system and parameter categories used in the analysis are presented in Table 2.

Rainfall maps were generated using annual rainfall data collected from seven meteorological stations located within and around the study area: Malang Climatology Station, Malang Geophysics Station, Pasuruan Geophysics Station, Nganjuk Geophysics Station, Juanda Meteorological Station, Perak I Meteorological Station, and Tanjung Perak Maritime Meteorological Station. Spatial interpolation was performed using the Kriging method in ArcGIS to produce the rainfall distribution map. Rainfall was assigned a 20% weight in the drought hazard analysis following the method proposed by Paimin et al. [20], as shown in Table 2.

Three land-use scenarios were used to evaluate drought distribution in the study area: Business as Usual (BAU), Regional Spatial Planning (RSP), and Land Capability Class (LCC). Land use was evaluated through a scoring approach with a weight of 15%, following the method of Paimin et al. [20], as presented in Table 2.

Data on dry months were obtained from the average number of dry months per year. Dry months are defined as months with rainfall below 150 mm. The number of dry months is one of the parameters contributing to drought vulnerability, which consists of five categories, was assigned a weight of 10% in the drought hazard analysis [20]. The dry-month is presented in Table 2.

Geological data were derived from geological map analysis of the study area. The geological parameter, classified into five categories, was assigned a weight of 10% in the drought hazard assessment [20]. Geological assessment is presented in Table 2.

The water use index (IPA) was used to evaluate water demand by comparing water requirements with available water resources. This index, a crucial factor in determining drought vulnerability, was derived from an analysis of water needs and potential. The water use index was calculated using Eq. (1).

$$IPA = \frac{Water\ Needs\ (m^3)}{Water\ Availability\ (m^3)} \quad (1)$$

Water needs and water availability were calculated according to Minister of Environment Regulation No. 17 of 2009, using Eq. (2) and Eq. (3).

a. Calculation of Water Needs (m^3/year)

$$Water\ needs = Total\ population \times The\ Need\ for\ Adequate\ Living\ Water \quad (2)$$

The need for adequate living water is equal to 1,600 m^3 of water per capita per year, which includes water for domestic purposes and food production.

b. Calculation of Water Availability (m^3/year)

$$Water\ Availability = 10\ x\ C\ x\ R\ x\ A \quad (3)$$

The value of C represents the weighted runoff coefficient, calculated using the Eq. (4).

$$C = \frac{\sum \quad c_i \times A_i}{\sum \quad A_i} \quad (4)$$

Where c_i is the runoff coefficient for land use type i, and A_i is the area of land use type i in hectares. R denotes the algebraic average of regional annual rainfall. A conversion factor of 10 is applied to convert the units from millimeters per hectare to cubic meters (m^3). The water use index was assigned a weight of 25% in the drought hazard assessment and consists of five categories [20]. The water use assessment is presented in Table 2.

Table 2. Categories and Scores based on Parameters

Parameter	Value	Category	Score
Annual Rainfall (mm)	>2000	Very Low	1
	1501-2000	Low	2
	1001-1500	Moderate	3
	500-1000	High	4
	<500	Very High	5
Land use	Protected Forest/Natural Forest	Very Low	1
	Production Forest	Low	2
	Shrub	Moderate	3
	Rice Field/Moor	High	4
	Residential Area	Very High	5
Dry Month	<2	Very Low	1
	3-4	Low	2
	5-7	Moderate	3
	7-8	High	4
	>8	Very High	5
Geology	Vulcan	Very Low	1
	Cmp Vulc-Folded Mountains	Low	2
	Folded Mountains	Moderate	3
	Sedimentary Rock	High	4
	Limestone Rock	Very High	5
Water Uses ($m^3.m^{-3}$)	<0.3	Very Low	1
	0.3 – 0.49	Low	2
	0.5 – 0.79	Moderate	3
	0.8 – 1.0	High	4
	>1.0	Very High	5
Specific Water Discharge ($m^3.s^{-1}.km^{-2}$)	>0.035	Very Low	1
	0.022 – 0.035	Low	2
	0.015 – 0.021	Moderate	3
	0.010 – 0.014	High	4
	< 0.010	Very High	5
Annual Evapotranspiration (mm)	<750	Very Low	1
	751 – 1000	Low	2
	1001 – 1500	Moderate	3
	1501 – 2000	High	4
	>2000	Very High	5

Specific water discharge was calculated using field observations and river discharge data collected from 27 observation points. The specific water discharge parameter was classified into five categories with a weight of 10% [20]. The specific water discharge assessment is presented in Table 2. Evapotranspiration data were obtained from secondary datasets and calculation methods based on climatic data. The evapotranspiration parameter was classified into five categories with a weight of 10%, following Paimin et al. [20], as presented in Table 2.

2.6 Potential Drought Hazard Analysis

Potential drought hazards were analyzed by calculating the score of each parameter included in the assessment, including average annual rainfall, land use, geology, number of dry months, specific water discharge, water use index, and annual evapotranspiration. Each parameter was assigned a score and weight. The final drought hazard index was calculated by summing the weighted scores, where the aspect value for each parameter was obtained by multiplying the score by its assigned weight. The total score was calculated using Eq. (5).

$$Total\ Score = \Sigma\ Weight\ x\ score \tag{5}$$

The classification of potential drought hazard levels is divided into five classes [20], as presented in Table 3.

Table 3. Classification of Potential Levels of Drought Hazards

Category	Value	Category
Very Low	> 4.3	Not Vulnerable
Low	3.5 – 4.3	A Bit Vulnerable
Moderate	2.6 – 3.4	Moderate
High	1.7 – 2.5	Vulnerable
Very High	< 1.7	Very Vulnerable

2.7 Accuracy Assessment

Accuracy assessment of the drought hazard map was conducted to evaluate the reliability of the resulting classification. The accuracy level was evaluated using overall accuracy based on field observation data. Overall accuracy was calculated as the number of correctly classified points divided by the total number of observation points.

$$Accuracy\ Assessment = \frac{\Sigma\ the\ point\ matches\ the\ result\ of\ observations}{Total\ Pont} \tag{6}$$

As shown in Eq. (6), overall accuracy was calculated as the ratio between the number of correctly classified points and the total number of observation points. The accuracy calculation followed the method proposed by Grandini et al. [21].

3. Result and Discussion

3.1 Historical Land Use and Land Cover Dynamics (2017–2025)

Land use and land cover patterns in the watershed changed subtstantially between 2017 and 2025 (Fig. 3). Natural forest declined from approximately 12,600.35 ha (31.4%) in 2017 to about 9,975.70 ha (24.9%) in 2025, representing a reduction of approximately 21%. Production forest also experienced a substantial decrease from 8,471.57 ha (21.1%) to 4,085.10 ha (10.2%) during the same period. In contrast, plantation areas expanded from 3,573.79 ha (8.9%) in 2017 to 7,196.73 ha (17.9%) in 2025, representing an increase of over 100%. Built-up areas increased from 3,457.39 ha (8.6%) to 4,650.07 ha (11.6%), indicating spatial expansion of settlements and infrastructure. Changes were also observed in shrubland, which expanded from 959.92 ha (2.4%) to 1,952.88 ha (4.9%), and rice fields, which increased from 936.30 ha (2.3%) to 1,373.38 ha (3.4%). These changes indicate a progressive conversion of forest areas into agricultural and managed land uses within the watershed.

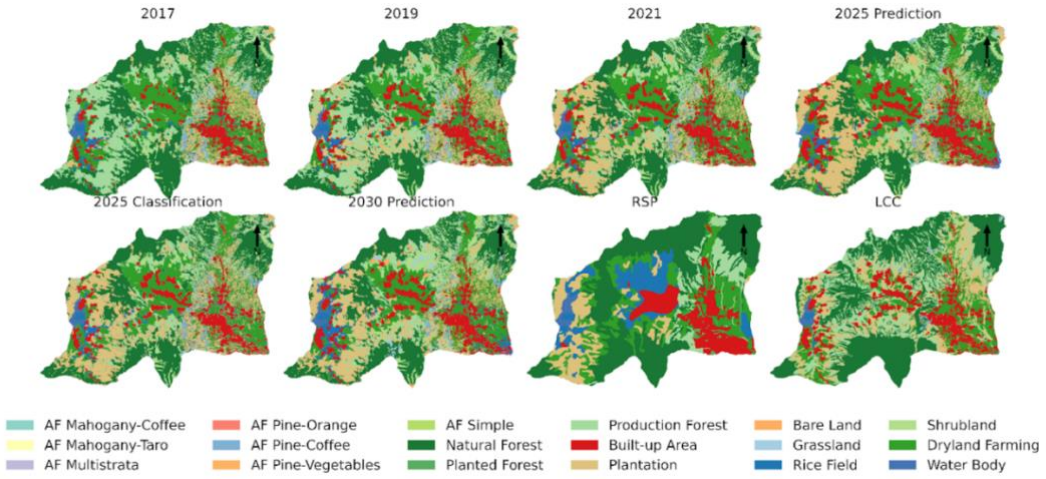

Fig. 3. Historical land use/land cover patterns in 2017, 2019, 2021, and 2025, the predicted 2025 map for model validation, and projected 2030 scenarios BAU, RSP, and LCC.

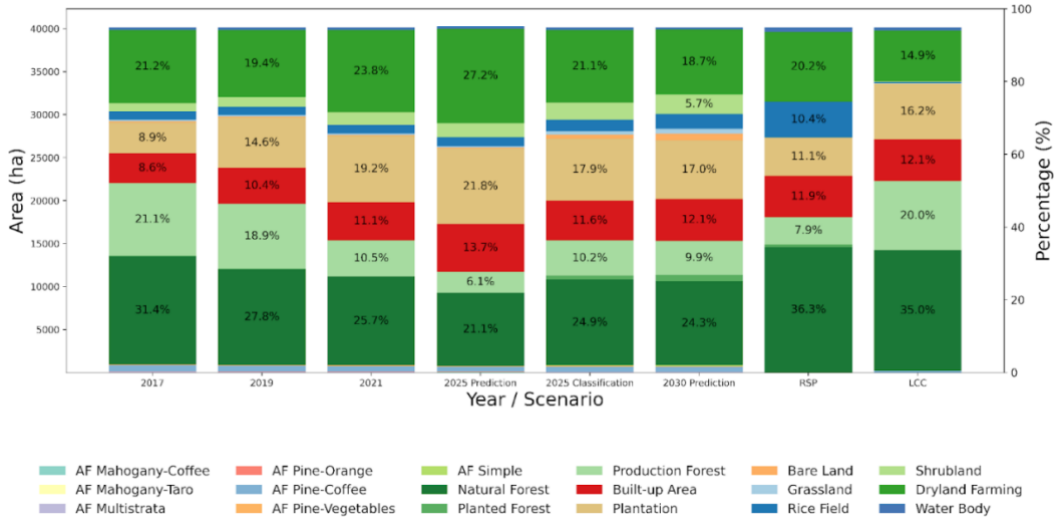

Fig. 4. Land-use composition and changes under historical and scenario-based conditions (2017–2030).

Overall, the observed period was characterized by increasing agricultural intensification and expansion of managed land uses. Plantation, dryland farming, and shrubland showed consistent growth, while natural forest and production forest exhibited sustained declines. The predicted 2025 land-use map reproduced the main spatial patterns of the classified 2025 dataset, although differences remained in plantation and natural forest areas. Model validation produced an overall accuracy of 0.783 and a Kappa coefficient of 0.737, indicating moderate agreement between predicted and observed maps. These results indicated that the ANN–CA–Markov model captured the main spatial dynamics of land-use change in the watershed.

Based on the calibrated model, projections for 2030 indicated continued expansion of several land-use types. Shrubland was projected to increase to 2,297.73 ha (5.7%), while rice fields were projected to expand to 1,711.55 ha (4.3%). Natural forest was projected to decline slightly to 9,769.68 ha (24.3%), and production forest was expected to stabilize at approximately 3,986.61 ha (9.9%). Plantation areas were projected to decrease slightly from 7,196.73 ha (17.9%) in 2025 to 6,815.72 ha (17.0%) in 2030, indicating partial redistribution to other agricultural or semi-natural land uses. The temporal trends are summarized in the stacked bar diagram in Fig. 4.

3.2 Land Use Transition and Model Validation for 2025

The transition matrix indicates that most land-use classes remained relatively stable between 2021 and 2025, although several notable transitions occurred among specific land-use categories. High persistence values were observed in several dominant land uses, particularly Natural Forest (0.957), Built-up Area (0.953), Plantation (0.897), Production Forest (0.874), and Dryland Farming (0.870), indicating that these land-use types experienced relatively limited changes during the observed period. However, certain land uses exhibited noticeable transitions to other categories. For example, [please define AF] Mahogany–Coffee retained 79.87% of its area, while portions transitioned to [AF] Pine–Coffee (0.064) and [AF] Pine–Orange (0.046). Similarly, [AF] Pine–Vegetables showed transitions toward Planted Forest (0.051) and [AF] Simple (0.052), indicating localized shifts in land management practices within the watershed.

Spatial changes were reflected in the differences between the observed 2021 land-use map and the predicted 2025 map. For instance, Natural Forest decreased from 1,535,160 pixels to 1,247,790 pixels, while Production Forest declined from 624,596 pixels to 358,456 pixels, indicating notable reductions in these land-use categories. In contrast, several land-use classes expanded during the modeled period. Built-up Area increased from 664,139 to 822,231 pixels, Plantation increased from 1,143,754 to 1,307,318 pixels, and Dryland Farming expanded from 1,420,461 to 1,631,446 pixels, reflecting spatial growth of these land uses within the watershed.

The performance evaluation of the model demonstrated a satisfactory level of accuracy in simulating land-use dynamics. The training process produced an accuracy of 0.7338, while comparison between predicted and reference maps produced an overall accuracy of 0.783 and a Kappa coefficient of 0.737. These results indicated that the model captured the dominant spatial patterns of land-use change.

3.3 Probability Maps of Land Use Change from the ANN Model

The ANN model generated spatial probability maps representing the likelihood of transition toward each land-use class as illustrated in Fig. 5. The resulting probability surfaces showed substantial variation among classes, with maximum probabilities reaching up to 0.9999 for several land-use types. Mean probability values varied across classes, ranging from 0.8658 for one class to below 0.03 for several others. For several classes, minimum probability values approach zero. These probability maps provided the spatial suitability input required for the Cellular Automata allocation process. Areas with higher probability values indicated locations with higher transition likelihood, while lower probabilities corresponded to more stable land-use conditions. The spatial probability layers were integrated with the transition probability matrix within the CA–Markov framework to guide the allocation of land-use changes during the simulation.

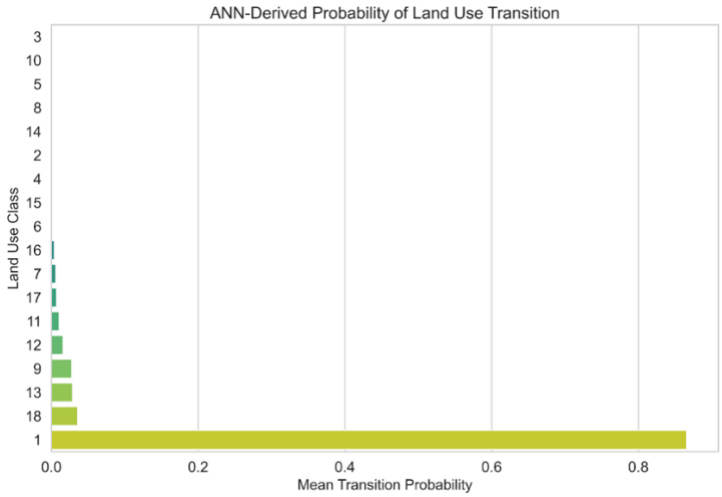

Fig. 5. Mean transition probability of land-use classes derived from the ANN model.

3.4 Land Use Scenario Comparison for 2030 (BAU), LCC, and RSP Scenarios

Land-use distribution was projected to 2030 under the business-as-usual (BAU), Regional Spatial Planning (RSP), and Land Capability Classification (LCC) scenarios using the calibrated ANN–CA–Markov model. The BAU projection indicated gradual changes among several land-use classes. Shrubland was projected to increase from 1,952.88 ha (4.9%) in 2025 to 2,297.73 ha (5.7%) in 2030, while rice fields were projected to expand from 1,373.38 ha (3.4%) to 1,711.55 ha (4.3%). In contrast, dryland farming was projected to decline from 8,458.03 ha (21.1%) to

7,516.95 ha (18.7%). Plantation areas were projected to decrease slightly from 7,196.73 ha (17.9%) to 6,815.72 ha (17.0%), while natural forest was projected to decline marginally from 9,975.70 ha (24.9%) to 9,769.68 ha (24.3%).

A comparison between the Regional Spatial Planning (RSP) and Land Capability Classification (LCC) scenarios showed differences in land allocation patterns (Fig. 3). Under the RSP scenario, natural forest occupied approximately 14,584.42 ha (36.5%), indicating a strong emphasis on forest conservation. In contrast, the LCC scenario allocated slightly less forest area at approximately 14,030.55 ha (35.1%). A major difference occurred in production forest, which reached 8,032.50 ha (20.1%) under the LCC scenario compared with 3,180.96 ha (8.0%) under the RSP scenario. Plantation areas also differed substantially between scenarios, covering 4,472.00 ha (11.2%) in the RSP framework but expanding to 6,501.75 ha (16.3%) under the LCC scenario. Agricultural land uses showed the opposite pattern. Rice fields reached 4,184.45 ha (10.5%) under the RSP scenario but declined sharply to only 133.85 ha (0.3%) under the LCC approach, reflecting differences in land allocation priorities.

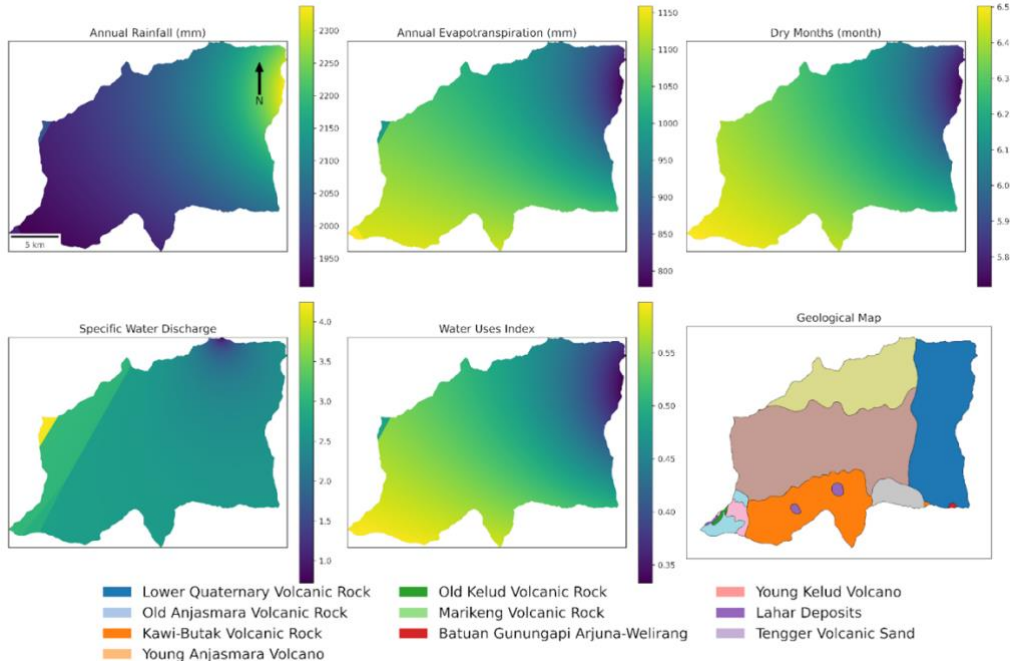

Fig. 6. Spatial distribution of climatic, hydrological, and geological parameters in the watershed.

3.5 Spatial Characteristics of Climatic, Hydrological, and Geological Parameters in the Watershed

Annual rainfall across the study area ranged from 1,865.63 to 2,773.34 mm, with a mean of 2,020.66 mm and a standard deviation of 115.97 mm (Fig. 6). The number of dry months varied between 5.00 and 6.69 months per year, with an average of 6.27 months and a standard deviation of 0.23 months. Annual evapotranspiration ranged from 428.91 to 1,376.93 mm, with a mean value

of 997.70 mm and a standard deviation of 105.93 mm. Specific water discharge ranged from 0.51 to 17.49 $m^3 s^{-1} km^{-2}$, with an average of 4.88 $m^3 s^{-1} km^{-2}$ and a standard deviation of 2.90 $m^3 s^{-1} km^{-2}$. The geological structure of the watershed was dominated by volcanic formations derived from several volcanic systems. The largest geological unit originated from the Anjasmara volcanic complex (153.05 km^2), followed by Arjuno–Welirang (96.02 km^2) and Kawi–Butak (63.30 km^2), with smaller deposits associated with the Kelud volcanic system.

3.6 Spatial Distribution of Drought Hazard at the Sub-catchment Level

The spatial distribution of drought hazard at the sub-catchment level changed between 2017 and 2030. In 2017, areas categorized as low drought hazard (Class 1) covered approximately 12,706.73 ha (31.9%), while moderate hazard (Class 2) dominated the watershed with 17,530.22 ha (44.0%), and high hazard areas (Class 3) occupied 9,588.98 ha (24.1%). By 2019, the extent of Class 1 decreased to 11,219.99 ha (28.2%), while Class 2 increased to 19,747.67 ha (49.6%). In 2021, Class 1 declined to 10,403.24 ha (26.1%), while Class 3 increased to 10,657.48 ha (26.8%) (Fig. 7).

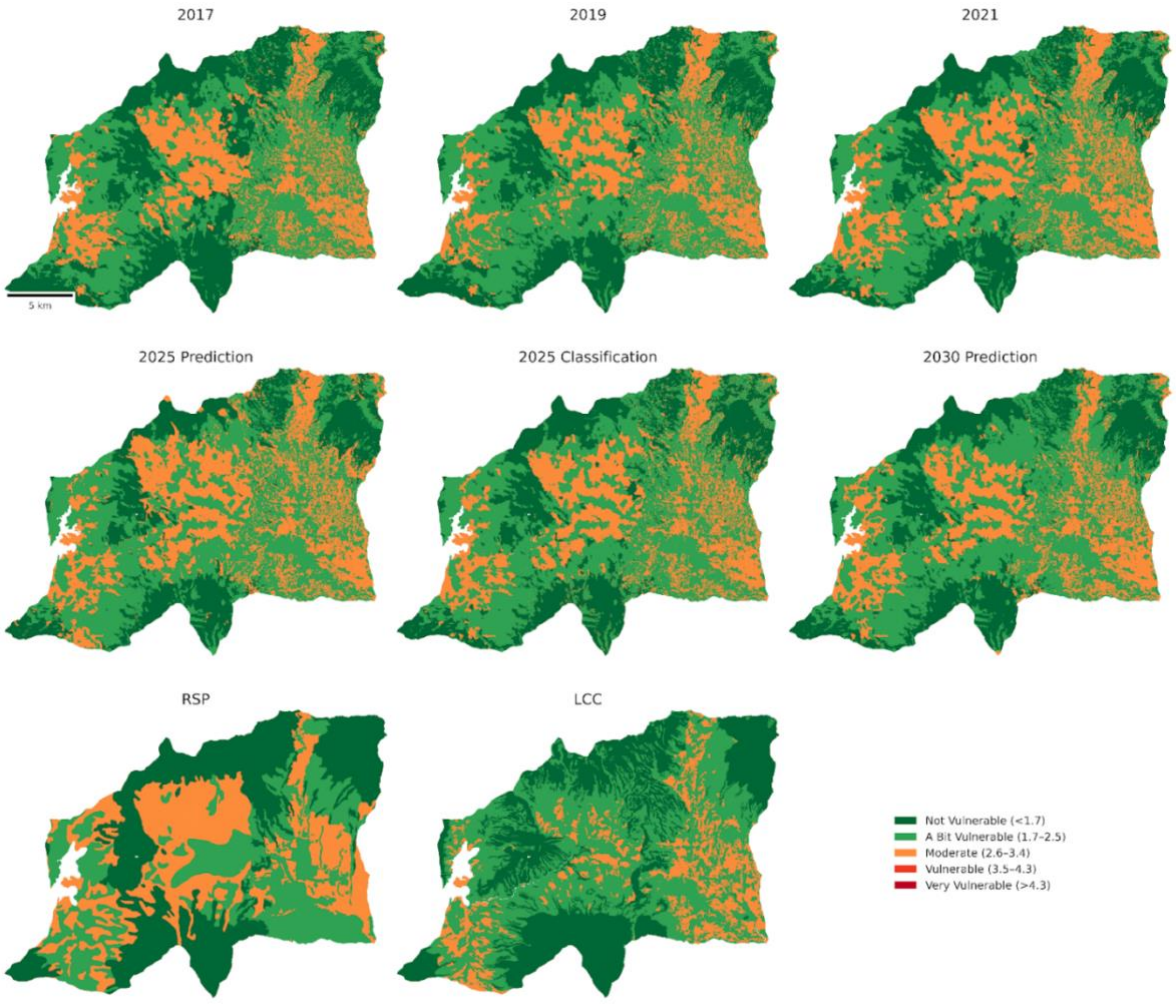

Fig. 7. Observed land use maps for 2017, 2019, and 2021, model-based prediction for 2025 and 2030, and scenario-based land use configurations (RSP, LCC).

Model projections indicated that this trend continued toward 2025 and 2030. The predicted 2025 scenario showed a reduction of Class 1 to 8,566.24 ha (21.5%), while Class 3 increased to 12,007.60 ha (30.2%). However, the classified 2025 map presented a slightly different distribution, with Class 1 covering 10,047.81 ha (25.2%), Class 2 dominating 19,476.13 ha (48.9%), and Class 3 occupying 10,300.06 ha (25.9%). By 2030, the model predicted that moderate drought hazard (Class 2) would remain dominant at 20,004.94 ha (50.2%), while Class 1 was projected to stabilize at approximately 9,824.34 ha (24.7%) and Class 3 at approximately 9,994.71 ha (25.1%). Model validation using field observations produced a Kappa coefficient of 0.8124.

3.7 Impact of Land Use Scenarios on Drought Hazard

The distribution of drought hazard under the 2030 Business-as-Usual (BAU), Regional Spatial Planning (RSP), and Land Capability Classification (LCC) scenarios differed across the watershed. Under the BAU scenario, moderate drought hazard (Class 2) dominated the landscape, covering approximately 20,004.94 ha (50.2%), while low hazard areas (Class 1) occupied about 9,824.34 ha (24.7%), and high hazard areas (Class 3) accounted for 9,994.71 ha (25.1%) (Fig. 8).

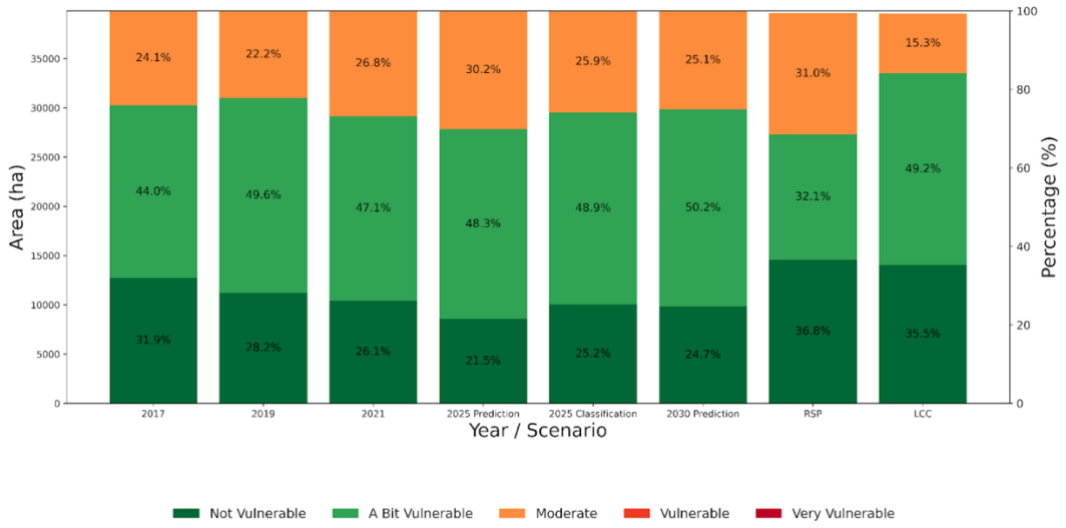

Fig. 8. Distribution of drought hazard classes (area in ha and percentage) across observed years (2017–2021), predicted conditions (2025 and 2030), and management scenarios (RSP, LCC).

In contrast, the RSP scenario showed a substantial increase in low drought hazard areas, reaching 14,586.27 ha (36.6%), while moderate hazard areas declined to 12,725.86 ha (32.0%), and high hazard areas covered 12,276.77 ha (30.8%). Meanwhile, the LCC scenario allocated 14,043.60 ha (35.3%) to low hazard areas and maintained a large extent of moderate hazard areas at 19,447.60 ha (48.8%), while high hazard areas decreased significantly to 6,063.43 ha (15.2%).

3.8 Land Use Transformation and Landscape Dynamics

The results indicated a gradual transformation of the watershed from a forest-dominated landscape toward more intensive agricultural and managed land uses, evidenced by a decline in natural forest from 12,600.35 ha (31.4%) in 2017 to 9,975.70 ha (24.9%) in 2025, together with a

reduction in production forest and expansion of plantation systems, agricultural land, and built-up areas. Overall, this represented a reduction of more than 20% of natural forest area in less than a decade. Such patterns are consistent with landscape intensification processes commonly observed in tropical regions [22], where economic pressures and land management decisions drive forest conversion [23]. As noted by Foley et al. [24], global land-use change is strongly linked to increasing demand for agricultural commodities and infrastructure, which often results in the replacement of natural ecosystems with managed landscapes. These changes can alter ecosystem functions, including hydrological regulation, soil stability, and carbon storage [25].

The expansion of plantation and agricultural systems observed in this study indicated a shift toward more commercially oriented land management. Lambin and Meyfroidt [26] explain that such transitions are often associated with broader socio-economic transformations, including market integration, technological development, and changing land management strategies. The simultaneous increase in shrubland and several agricultural categories suggested that land-use change may occur through intermediate stages rather than direct conversion from forest to permanent cultivation [27]. This transitional landscape structure reflects the interaction between ecological processes, economic incentives, and land management decisions in shaping land-use dynamics within the watershed [28].

3.9 Implications of Land Use Change for Drought Hazard

Changes in land-use composition in the watershed were associated with shifts in drought hazard patterns across sub-catchments. The results indicated that moderate drought hazard areas increasingly dominated the watershed, while higher hazard areas expanded in several sub-catchments. In this study, moderate drought hazard increased from 44.0% of the watershed area in 2017 to approximately 50.2% under the projected 2030 BAU scenario.

These patterns suggest that land-use transformation influences watershed hydrological processes [29]. Vegetation structure, rooting depth, and soil cover influence soil moisture retention, evapotranspiration, and infiltration capacity, which regulate drought vulnerability at the watershed scale [30]. As emphasized by Wu et al. [31], forest ecosystems contribute substantially to hydrological buffering by enhancing infiltration and maintaining soil moisture storage, whereas the conversion of forests into agricultural or plantation systems can alter these processes and increase the sensitivity of landscapes to climatic variability.

The expansion of plantation and agricultural land uses may therefore contribute to shifts in drought hazard by modifying vegetation characteristics and soil–water interactions. According to Awhari et al. [32], large-scale conversion of natural vegetation to plantation systems can significantly alter watershed hydrology by influencing evapotranspiration and water availability

[33]. These findings suggest that the spatial redistribution of drought hazard observed in this study may not solely reflect climatic variability but also the cumulative impact of land-use transitions on watershed-scale water balance and ecosystem functioning.

3.10 Effectiveness of Scenario-Based Land Use Planning for Drought Mitigation

The comparison of land-use scenarios highlighted the role of spatial planning and land suitability in shaping future drought vulnerability across the watershed. The business-as-usual (BAU) scenario reflected the continuation of existing land-use trajectories, where agricultural expansion and mixed land management maintained moderate drought susceptibility across large portions of the watershed. For example, high drought hazard areas declined from 25.1% under the BAU scenario to 15.2% under the LCC scenario. Such trajectories are commonly observed in rapidly developing rural regions, where land-use decisions are often driven by short-term economic incentives. As noted by Verburg et al. [34], scenario-based land-use modeling provides an important tool for understanding how alternative policy and management strategies may influence future landscape configurations and associated environmental risks.

The alternative scenarios examined in this study demonstrated that spatial planning and land capability–based allocation could significantly influence drought hazard patterns. The Regional Spatial Planning (RSP) scenario prioritized forest conservation and regulated land development, maintaining greater vegetation cover within the watershed [35]. In contrast, the Land Capability Classification (LCC) scenario aligned land use more closely with biophysical suitability, promoting land uses compatible with soil characteristics, terrain conditions, and hydrological constraints [36]. These findings suggest that integrating land capability assessment with spatial planning frameworks may provide an effective strategy for balancing agricultural development, forest conservation, and watershed resilience under future environmental change.

Overall, the results demonstrate a strong linkage between land-use dynamics and drought vulnerability at the watershed scale. The transformation of forest-dominated landscapes into agricultural, plantation, and settlement systems alters vegetation structure, soil–water interactions, and evapotranspiration processes that regulate watershed hydrological responses. As emphasized by Bruijnzeel [37], forest ecosystems play a crucial role in maintaining watershed hydrological stability, whereas the conversion of natural vegetation into simplified land-use systems may reduce this buffering capacity. The scenario analysis further indicated that integrating land capability assessment with spatial planning could guide landscape development toward more sustainable land-use configurations while reducing drought risk. These findings highlight the importance of combining land capability evaluation, spatial planning strategies, and watershed management to support climate-resilient landscape development in tropical watersheds.

4. Conclusions

This study demonstrates that land-use change significantly shapes drought hazard patterns within tropical watershed systems. Between 2017 and 2025, natural forest declined from 12,600.35 ha (31.4%) to 9,975.70 ha (24.9%), a reduction of more than 20%, accompanied by the expansion of plantation systems, agricultural land, and built-up areas. These transformations reflect ongoing landscape intensification driven by agricultural development and land management decisions.

The results showed that such changes were associated with shifts in drought hazard patterns across sub-catchments, where moderate drought hazard increased from 44.0% of the watershed area in 2017 to approximately 50.2% under the projected 2030 Business-as-Usual (BAU) scenario. Changes in vegetation structure and land management practices influence soil moisture retention, evapotranspiration, and infiltration processes, thereby affecting the hydrological buffering capacity of the watershed.

Scenario-based simulations further demonstrate that alternative land-use planning strategies can significantly influence future drought risk patterns. While the BAU scenario maintained moderate drought susceptibility across much of the watershed, the Regional Spatial Planning (RSP) scenario increased low drought hazard areas through stronger forest protection, and the Land Capability Classification (LCC) scenario showed the greatest potential for drought mitigation by reducing high drought hazard areas from 25.1% under BAU to 15.2%.

These findings highlight the importance of integrating land capability assessment with spatial planning to guide sustainable land-use development. Aligning land use with environmental capacity can reduce drought vulnerability while maintaining agricultural productivity and ecosystem stability, providing an important pathway for climate-resilient watershed management in tropical regions.

Abbreviations

CA-ANN	Cellular Automata - Artificial Neural Network
LCC	Land Capability Class
RSP	Regional Spatial Planning
BAU	Business As Usual
AF	Agroforestry
IPA	Indeks Penggunaan Air *(Water Use Index)*
MOLUSCE	Modules for Land Use Change Simulations
GDAL	Geospatial Data Abstraction Library
DOS	Dark Object Subtraction

Data availability statement

Data will be shared upon request by the readers

CRediT authorship contribution statement

Suryanta Junjungan Tua Sitioa: Data curation, Formal analysis, Investigation, Methodology, Writing – original draft. **Novandi Rizky Prasetya:** Formal analysis, Validation, Writing – review and editing. **Michelle Talisia Sugiarto:** Writing – review and editing. **Aditya Nugraha Putra**: Conceptualization, Data curation, Formal analysis, Funding acquisition, Investigation, Methodology, Project administration, Resources, Software, Supervision, Validation, Visualization, Writing – original draft, Writing – review and editing.

Declaration of Competing Interest

The authors of this manuscript declare no conflict of interest or competing interest

Declaration of Use of AI in the Writing Process

The author(s) used ChatGPT (OpenAI) during the preparation of this manuscript to improve grammar and language quality. After using the tool, the author(s) carefully reviewed and edited the content and take full responsibility for the content of the publication.

Acknowledgement

This research was supported by the PNBP Fund of the Faculty of Agriculture, Brawijaya University, Indonesia. We acknowledge the assistance provided in language editing, formatting, and proofreading during the preparation of this manuscript. The funders had no role in study design, data collection and analysis, decision to publish, or preparation of the manuscript.

References

[1] Pizzorni M, Innocenti A, Tollin N. Droughts and floods in a changing climate and implications for multi-hazard urban planning: A review. City and Environment Interactions 2024;24:100169. https://doi.org/10.1016/j.cacint.2024.100169.

[2] Gunawan H, Mulyanto B, Suharti S, Subarudi S, Ekawati S, Karlina E, et al. Forest land redistribution and its relevance to biodiversity conservation and climate change issues in Indonesia. Forest Sci Technol 2024;20:213–28. https://doi.org/10.1080/21580103.2024.2347902.

[3] Haryanto Yd, Budiprabowo Na. Sebaran Spasial Wilayah Rawan Kekeringan Lahan Tanaman Padi Sebagai Upaya Manajemen Risiko Bencana Kekeringan Di Provinsi Jawa Timur. Jurnal Manajemen Bencana (Jmb) 2022;8. https://doi.org/10.33172/jmb.v8i1.745 https://www.academia.edu/122084627/Sebaran_Spasial_Wilayah_Rawan_Kekeringan_Lahan_Tanaman_Padi_Sebagai_Upaya_Manajemen_Risiko_Bencana_Kekeringan_DI_Provinsi_Jawa_Timur

[4] Rahma AD, Rosidi M, Zapariza R, Sulaeman E, Ridwan I. Infiltration ability in the area of land use change, Bogor, West Java. Appl Water Sci 2023;13:213. https://doi.org/10.1007/s13201-023-02015-z.

[5] Waskitho NT. Model Budaya Organisasi Dalam Pengelolaan Daerah Aliran Sungai Brantas Model of Organizational Culture in Watershed Management Brantas 8 https://media.neliti.com/media/publications/11418-ID-model-budaya-organisasi-dalam-pengelolaan-daerah-aliran-sungai-brantas.pdf

[6] Pandit A, Batelaan O, Pandey VP, Adhikari S. Depleting spring sources in the Himalayas: Environmental drivers or just perception? J Hydrol Reg Stud 2024;53:101752. https://doi.org/10.1016/j.ejrh.2024.101752.
[7] Yang D, Yang Y, Xia J. Hydrological cycle and water resources in a changing world: A review. Geography and Sustainability 2021;2:115–22. https://doi.org/10.1016/j.geosus.2021.05.003.
[8] Wirosoedarmo R, Haji ATS, Zulfikar F. Analisa Perubahan Tata Guna Lahan dan Pengaruhnya Terhadap Pencemarandi Brantas Hulu, Kota Batu, JawaTimur. Jurnal Sumberdaya Alam Dan Lingkungan 2016;3:33–9. https://jsal.ub.ac.id/index.php/jsal/article/view/251
[9] Li S, Sparrow SN, Otto FEL, Rifai SW, Oliveras I, Krikken F, et al. Anthropogenic climate change contribution to wildfire-prone weather conditions in the Cerrado and Arc of deforestation. Environmental Research Letters 2021;16:094051. https://doi.org/10.1088/1748-9326/ac1e3a.
[10] Haris FD, Sitorus SRP, Tjahjono B. Kesesuaian Rencana Tata Ruang Wilayah (RTRW) berbasis bahaya banjir menggunakan analisis hierarki proses di Kabupaten Kuningan. Region : Jurnal Pembangunan Wilayah Dan Perencanaan Partisipatif 2022;17:124. https://doi.org/10.20961/region.v17i1.44172.
[11] Hermans K, McLeman R. Climate change, drought, land degradation and migration: exploring the linkages. Curr Opin Environ Sustain 2021;50:236–44. https://doi.org/10.1016/j.cosust.2021.04.013.
[12] Zhu Z, Qiu S, Ye S. Remote sensing of land change: A multifaceted perspective. Remote Sens Environ 2022;282:113266. https://doi.org/10.1016/j.rse.2022.113266.
[13] Setiawan B, Aditya Nugraha Putra dan. Pemetaan Daerah Rawan Longsor Di Kecamatan Pujon Menggunakan Metode Analytic Hierarchy Process (AHP) 2017;4: 567-76. https://jtsl.ub.ac.id/index.php/jtsl/article/view/174/pdf
[14] Page BP, Olmanson LG, Mishra DR. A harmonized image processing workflow using Sentinel-2/MSI and Landsat-8/OLI for mapping water clarity in optically variable lake systems. Remote Sens Environ 2019;231:111284. https://doi.org/10.1016/j.rse.2019.111284.
[15] White L, Millard K, Banks S, Richardson M, Pasher J, Duffe J. Moving to the RADARSAT Constellation Mission: Comparing Synthesized Compact Polarimetry and Dual Polarimetry Data with Fully Polarimetric RADARSAT-2 Data for Image Classification of Peatlands. Remote Sens (Basel) 2017;9:573. https://doi.org/10.3390/rs9060573.
[16] Topaloğlu RH, Sertel E, Musaoğlu N. Assessment Of Classification Accuracies Of Sentinel-2 And Landsat-8 Data For Land Cover / Use Mapping. Isprs - International Archives of the Photogrammetry, Remote Sensing and Spatial Information Sciences 2016;XLI-B8:1055–9. https://doi.org/10.5194/isprsarchives-XLI-B8-1055-2016.
[17] Zhang H, Xin M, Wang B, Wang J, Lin C, Gu X, et al. Spatiotemporal variations in phosphorus concentrations in the water and sediment of Jiaozhou Bay and sediment phosphorus release potential. Science of The Total Environment 2022;806:150540. https://doi.org/10.1016/j.scitotenv.2021.150540.
[18] Putra AN, Nita I, Wicaksono KS, Prasetya NR, Sugiarto MT, Hidayat F, et al. Potential erosion and sedimentation based on land use change by using cellular automata-artificial neural network. Geomatics, Natural Hazards and Risk 2025;16. https://doi.org/10.1080/19475705.2025.2461058.
[19] Quandt A, Herrick J, Peacock G, Salley S, Buni A, Mkalawa CC, et al. A standardized land capability classification system for land evaluation using mobile phone technology. J Soil Water Conserv 2020;75:579–89. https://doi.org/10.2489/jswc.2020.00023.
[20] Pramono IBudi, Indrawati DRetna. Sistem perencanaan pengelolaan daerah aliran sungai 2013:100. https://tile.loc.gov/storage-services/service/gdc/gdcovop/2012330829/2012330829.pdf

[21] Grandini M, Bagli E, Visani G. Metrics for Multi-Class Classification: an Overview. A White Paper 2020. https://arxiv.org/abs/2008.05756
[22] Babatunde CA, Abdulraheem MI, Aruleba JO, Nurudeen OO, Ande OT, Afolabi OM. Soil Color Indicators of Biogeochemical Changes Under Land Use Intensification in Tropical Climosequences. n.d. 2026;8: 38-55 https://www.researchgate.net/publication/401038399_Soil_Color_Indicators_of_Biogeochemical_Changes_Under_Land_Use_Intensification_in_Tropical_Climosequences
[23] Risnawati D. Emerging Trends and Knowledge Structure in Indonesian Forest Management: A Bibliometric Analysis. Forest and Nature 2026;2:28–41. https://doi.org/10.63357/fornature.v2i1.33.
[24] Foley JA, DeFries R, Asner GP, Barford C, Bonan G, Carpenter SR, et al. Global Consequences of Land Use. Science (1979) 2005;309:570–4. https://doi.org/10.1126/science.1111772.
[25] Umwali ED, Isabwe A, Kayitesi NM, Chen X. Bi-decadal changes in selected ecosystem services and their integrated drivers in East Africa. Global Environmental Change 2026;97:103115. https://doi.org/10.1016/j.gloenvcha.2026.103115.
[26] Lambin EF, Meyfroidt P. Global land use change, economic globalization, and the looming land scarcity. Proceedings of the National Academy of Sciences 2011;108:3465–72. https://doi.org/10.1073/pnas.1100480108.
[27] Woldearegay M, Woldu Z, Masresha G, Samuel Y. Land use/land cover change dynamics of moist evergreen afromontane forest, Southern Ethiopia: Implications for conservation. Sci Afr 2026;31:e03204. https://doi.org/10.1016/j.sciaf.2026.e03204.
[28] Hotz R, Brown C, Zeng Y, Schmitt T, Rounsevell M. Modelling Socio-Psychological Drivers of Land Management Intensity 2026. https://www.researchgate.net/publication/400395733_Modelling_Socio-Psychological_Drivers_of_Land_Management_Intensity
[29] Gidey E, Birhane E, Mhangara P, Akalu F, Nasir J, Hishe S, et al. Modeling future land use and land cover change and hydrological implications in the Dabus watershed of southwest Ethiopia. Discover Geoscience 2026;4:28. https://doi.org/10.1007/s44288-026-00399-4.
[30] Yan Q-S, Peng Y-X, Jiang X-J, Fu P-L, Lu Z-Y, Hu X-W, et al. Soil moisture dynamics and rainfall infiltration across vegetation types in subtropical ecosystems in Southwest China. Catena (Amst) 2026;262:109693. https://doi.org/10.1016/j.catena.2025.109693.
[31] Wu Y, Yu X, Jia G, Liu Z, Rao H. Response of hydrological processes to event- and annual-scale precipitation extremes in a rocky mountainous area of northern China. Catena (Amst) 2026;264:109803. https://doi.org/10.1016/j.catena.2026.109803.
[32] Awhari DP, Jamal MH Bin, Muhammad MKI, Nasara MA, adi ZS, Shiruf MS, et al. Future Cropland Exposure to Drought Frequency Under Climate Change and Land-Use Scenarios in Nigeria. Earth Systems and Environment 2026. https://doi.org/10.1007/s41748-025-01015-0.
[33] Fu C, Song X, Li H. Estimation of the monthly change in soil water storage in two watersheds of contrasting vegetation cover. Catena (Amst) 2026;266:109925. https://doi.org/10.1016/j.catena.2026.109925.
[34] VERBURG PH, NEUMANN K, NOL L. Challenges in using land use and land cover data for global change studies. Glob Chang Biol 2011;17:974–89. https://doi.org/10.1111/j.1365-2486.2010.02307.x.
[35] Liu M, Liu S, Tang R, Liu M, Hu X, Lin S, et al. Identification of forest priority conservation and restoration areas for different SSPs-RCPs scenarios. J Environ Manage 2025;375:124412. https://doi.org/10.1016/j.jenvman.2025.124412.
[36] Tahir Z, Haseeb M, Mahmood SA, Batool S, Abdullah-Al-Wadud M, Ullah S, et al. Predicting land use and land cover changes for sustainable land management using CA-

Markov modelling and GIS techniques. Sci Rep 2025;15:3271. https://doi.org/10.1038/s41598-025-87796-w.

[37] Bruijnzeel LA. Hydrological functions of tropical forests: not seeing the soil for the trees? Agric Ecosyst Environ 2004;104:185–228. https://doi.org/10.1016/j.agee.2004.01.015.